Neurochemistry International 191 (2025) 106084

Contents lists available at ScienceDirect

Neurochemistry International

journal homepage: www.elsevier.com/locate/neuint

Functional impact of CYFIP2 RNA editing on actin regulation, axon growth, and spinogenesis

Luca La Via [a], Elona Ndoj [a], Matteo Bertoli [a], Veronica Mutti [a], Giulia Carini [a], Alice Filippini [a,b], Federica Bono [a], Chiara Fiorentini [a], Giovanni Ribaudo [a], Alessandra Gianoncelli [a], Giuseppe Borsani [a], Isabella Russo [a,b], Alessandro Barbon [a,c,d,*]

[a] Department of Molecular and Translational Medicine, University of Brescia, Brescia, Italy
[b] Genetics Unit, IRCCS Istituto Centro San Giovanni di Dio Fatebenefratelli, Brescia, Italy
[c] Consorzio Interuniversitario Biotecnologie, Trieste, Italy
[d] CSGI, Center for Colloid and Surface Science, Florence, Italy

ARTICLE INFO

Keywords:
RNA editing
CYFIP1
CYFIP2
Actin
FMRP

ABSTRACT

Cytoplasmic FMRP-interacting protein 2 (CYFIP2) is a component of the wave regulatory complex (WRC), one of the most important players in regulating cellular actin dynamics. Interestingly, the CYFIP2 transcript undergoes RNA editing, an epitranscriptomic modification catalyzed by ADAR enzymes, which leads to adenosine (A) to inosine (I) deamination. *CYFIP2* editing in the coding sequence results in a K/E substitution at amino acid 320. The functional meaning of this regulation is still unknown. In this study, we aimed to investigate the potential implications of CYFIP2 RNA editing related to actin dynamics during cell differentiation, axon development and synaptogenesis in neural cells. We generated SH-SY5Y neuroblastoma cell lines in which the *CYFIP2* gene has been functionally inactivated via CRISPR-Cas9 technology. *CYFIP2* KO cells exhibited profound actin filament disorganization and loss of the ability to differentiate into a neuron-like phenotype. The overexpression of both the unedited (K) and edited (E) CYFIP2 isoforms restored normal abilities. Finally, we used primary neuronal cultures in which endogenous CYFIP2 was knocked down via short hairpin RNA (shRNA) technology and *CYFIP2* editing variants were overexpressed.

While CYFIP2-KD cells presented a decrease in axon development and spine frequency, CYFIP2-E variants increased the number of axon branches, total axon length and dendritic spine frequency compared with both CYFIP2-KD cells and CYFIP-K variants. Overall, our work reveals for the first time the functional significance of the CYFIP2 K/E RNA editing process in regulating the spread of neuronal axons during the initial stages of in vitro development and spinogenesis.

1. Introduction

A variety of eukaryotic cell characteristics, including cell shape, migration and vesicle trafficking, are driven by the dynamic rearrangement of the actin cytoskeleton (Pollard, 2016). The coordination of actin filament dynamics is crucial for the development, maturation, and function of neurons, one of the most remarkable examples of cellular polarization (Konietzny et al., 2017). Moreover, the remodeling of the underlying actin cytoskeleton determines how dendritic spine size and shape vary in relation to excitatory synapse functions. Spine development, plasticity and synaptic function all depend on actin dynamics (Citri and Malenka, 2008). In addition to synaptic impacts, the regulation of actin cytoskeleton dynamics is essential for the development of brain circuit complexity, as it modifies and guides the extension of axonal projections from neurons to their specific destinations for synaptic connections (Omotade et al., 2017).

Cytoplasmic FMRP-interacting proteins (CYFIPs) are part of the Wiscott–Aldrich syndrome protein family verprolin-homologous protein (WAVE)-related complex (WRC), one of the most important players that regulate cellular actin dynamics. In the basal state, the WRC is inhibited by CYFIPs because of the sequestration of the activity-bearing Verprolin-Homologous, Central, Acidic (VCA) domain of WAVE. Binding of the active form of the small GTPase RAC1 to CYFIPs induces conformational changes in the WRC, which releases the VCA domain to trigger ARP2/3-

* Corresponding author. Department of Molecular and Translational Medicine, University of Brescia, Brescia, Italy.
E-mail address: alessandro.barbon@unibs.it (A. Barbon).

https://doi.org/10.1016/j.neuint.2025.106084
Received 8 May 2025; Received in revised form 20 October 2025; Accepted 4 November 2025
Available online 5 November 2025

induced actin polymerization (Chen et al., 2010). Accordingly, the WRC signaling pathway plays a crucial role in important neurodevelopmental processes such as axon guidance and synapse morphology.

The two family members CYFIP1 and CYFIP2, in addition to being part of the WRC, might interact with fragile X-messenger ribonucleoprotein (FMRP), an RNA-binding protein with an important role in translational control, the lack of which leads to fragile X syndrome (FXS) (Schenck et al., 2001). These two proteins are highly similar and conserved in several organisms (Zhang et al., 2018) and share 99 % identity with their orthologs in mice (Schenck et al., 2001). Among these proteins, CYFIP1 has been extensively studied and plays an important role in neurodevelopment by linking FMRP-dependent local translation with signaling-dependent actin remodeling through the WRC (Schenck et al., 2003). Owing to their high sequence similarity, CYFIP1 and CYFIP2 may share common functions. However, CYFIP1 is expressed in most tissues, whereas CYFIP2 is highly expressed in the brain; furthermore, in the brain, CYFIP1 is expressed by nonneuronal cells, whereas CYFIP2 is more enriched in neurons than in other cell types (Zhang et al., 2019). Recently, de novo CYFIP2 mutations have been identified in patients with neurodevelopmental disorders (Zhang et al., 2019; Kang et al., 2023; Ma et al., 2025). Finally, CYFIP2 function can be regulated at the co-transcriptional level by RNA editing, a mechanism mediated by adenosine deaminases that act on RNA (ADARs) (Orlandi et al., 2012). ADAR enzymes are responsible for the modification of adenosine (A) into inosine (I). Considering that I can be read as G by the ribosome, A-to-I editing can change the amino acid insertion during translation. RNA editing in CYFIP2 results in a K320E substitution, which mainly occurs in the brain. At the protein level, the editing-dependent amino acid change is located between the WAVE1 interaction domain and the FMRP interaction domain, and this modification is conserved across different species, highlighting a functional relevance that has never been investigated (Levanon et al., 2005).

Here, we aimed to investigate the biological implications of *CYFIP2* RNA editing related to actin dynamics during axon development and synaptogenesis in neural cells. Understanding the role of the CYFIP2 RNA editing substitution would be fundamental for further analysis in both normal and pathological brains.

2. Materials and methods

2.1. SH-SY5Y culture and differentiation

The human neuroblastoma SH-SY5Y cell line was purchased from the American Tissue Culture Collection (ATCC™, CRL2266). The cell lines were grown in a 1:1 mixture of Ham's F12 Nutrient Mix (Thermo Fisher Scientific) and Dulbecco's modified Eagle's medium (DMEM, Merck) supplemented with high glucose (4.5 g/L), L-glutamine 4 mM (Thermo Fisher Scientific) and sodium pyruvate 1 mM (Thermo Fisher Scientific). The medium was supplemented with 10 % v/v heat-inactivated fetal bovine serum (FBS, Thermo Fisher Scientific) and penicillin–streptomycin 1 % solution (P/S, Merck). The cells were cultivated at 37 °C with 5 % CO2 at saturated humidity and kept below ATCC passage +15 to avoid cell senescence. To differentiate SH-SY5Y cells, a two-step retinoic acid (RA, Thermo Fisher Scientific) and brain-derived neurotrophic factor (BDNF, Merck) protocol was used (Hromadkova et al., 2020). In brief, cells were seeded at a density of 1×10^4 cells/cm^2 on poly-D-lysine (Merck) precoated slides. The cells were grown in RALS medium (DMEM/F12 1:1; FBS 3 %; P/S; L-glutamine 4 mM; RA 10 μM). After 6 days, the culture medium was replaced with RANBB medium (NeuroBasal medium; B27; (Thermo Fisher Scientific) P/S; L-glutamine 4 mM; RA 10 μM; BDNF 50 ng/ml) for another six days of culture. The culture medium was changed every two days.

2.2. Primary hippocampal neuronal culture maturation and drug treatments

All experiments complied with the guidelines for the use of experimental animals issued by the European Community Council Directive 86/609/EEC and were approved by the Italian Ministry of Health (ID: 480/2017). Primary hippocampal neurons were prepared as described in Mingardi et al. (2021). Briefly, pregnant mice were killed by cervical dislocation and hippocampi from embryos at day 16.5 were dissociated mechanically, and neurons were resuspended in Neurobasal™ medium (Thermo Fisher Scientific) supplemented with B27 (Thermo Fisher Scientific) containing 30 U/ml penicillin, streptomycin 30 mg/mL, GlutaMAX 0.75 mM (Thermo Fisher Scientific) and L-glutamine 0.75 mM. Neurons were seeded at a density of 40.000 cells/cm^2 on precoated poly-D-lysine 0.1 mg/mL glass coverslips or 25.000 cells/cm^2 in poly--D-lysine-coated 0.02 mg/ml 6-well plates and maintained at 37 °C under a 5 % CO2 humid atmosphere. Three days after seeding, half of the medium was replaced with 24-h astrocyte-conditioned medium. Furthermore, half of the medium was changed every seven days up to a maximum of four weeks. Various long-term pharmacological treatments were applied to hippocampal neuronal cell growth in 6-well plates at day in vitro (DIV) 14. KCl 25 mM (Merck) and glutamate 50 μM (Merck) (Bonini et al., 2015). (2R)-amino-5-phosphonovaleric acid 100 μM (APV, Merck) in combination with tetrodotoxin 1 μM (TTX, Merck) (Orlandi et al., 2011); chemical long-term potentiation (cLTP, forskolin 50 μM (Merck), picrotoxin 100 μM (Merck), Rolipram 100 nM (Merck), BDNF 50 ng/ml) (Otmakhov et al., 2004); or chemical long-term depression (cLTD, (S)-3,5-Dihydroxyphenylglycine 25 μM (DHPG, Merck)) (Snyder et al., 2001). After 24 h of treatment, the cells were harvested, and total RNA was extracted to evaluate the RNA editing level of the *CYFIP2* transcript. The cells that grew on glass slides were used for live imaging microscopy at DIV4 or fixed for 20 min with a 4 % paraformaldehyde (Merck) solution in PBS for use in fluorescence microscopy.

2.3. Molecular modeling

The structures of the WAVE complexes, in their active and inactive forms, were retrieved from the Protein Data Bank (PDB, rcsb.org, accessed on Jan 15, 2025). In particular, models of the cryo-EM structure of the WAVE regulatory complex with Rac1 bound to both the A and D sites at a resolution of 3.00 Å (active, PDB ID 7USE) and of the cryo-EM structure of the WAVE regulatory complex at a resolution of 3.00 Å (inactive, PDB ID 7USC) were used (Ding et al., 2022). CYFIP1 was manually removed from such structures via UCSF Chimera 1.17.1 (Pettersen et al., 2004).

The model of CYFIP2 was generated via AlphaFold (AF-Q96F07–F1-v4, UniProt Q96F07) (Jumper et al., 2021; Varadi et al., 2022). The K320E variant was produced with UCSF Chimera 1.17.1 via the *swapaa* command, which includes the Rotamers tool that allows the optimization of side chain orientation (Pettersen et al., 2004). The Dock Prep tool was then used to prepare all the proteins before docking, particularly to fix missing side chains and to add hydrogens and charges under the AMBER ff14SB forcefield. The protein–protein docking experiments were performed via the HDOCK server (hdock.phys.hust.edu.cn, accessed on Jan 15, 2025) (Yan et al., 2020), which is based on a hybrid algorithm of template-based modeling and *ab initio* free docking. According to the docking algorithm, the protein defined as the "ligand" is rotated and translated, and the top 10 translations for each rotation are optimized by the iterative knowledge-based scoring function. The binding modes to the protein defined as the "receptor" are then clustered with a root mean square deviation (RMSD) cutoff of 5 Å. Modified WAVE complexes, in which CYFIP1 was removed, and CYFIP2 variants are uploaded to the HDOCK server as receptor and ligands, respectively, for the docking experiments performed via default settings. After the calculations, the docked structures and the resulting files were retrieved

and processed via UCSF Chimera 1.17.1, which was also used to produce the artworks (Pettersen et al., 2004). The scores obtained from the docking studies were expressed in -kcal/mol.

2.4. Total RNA isolation, reverse transcription and sequencing

Neuronal cultures at different DIVs or cell cultures (A-172; HeLa; HEK293T; SH-SY5Y) were washed with RNase-Free PBS and mechanically harvested in 1 mL of TRIzol™ (Thermo Fisher Scientific), and total RNA was extracted with a Direct-zol™ RNA miniprep kit (Zymo Research) following the manufacturer's instructions. The concentration of the eluted RNA was measured on a Nanodrop™ ND-1000 Spectrophotometer (Thermo Fisher Scientific). The poly-A^+ mRNA samples from different brain areas (Cc-corpus callosum; Hi-hippocampus; Nc-caudate nucleus; Sc-spinal cord; thalamus; and Cx-cerebral cortex) were derived from the brain pools of 19 normal male/female Caucasians (Clontech). One microgram of total RNA from cell cultures or 50 ng of poly-A^+ mRNA from human brain tissues was reverse transcribed via Moloney murine leukemia virus reverse transcriptase (M-MLV RT) (Thermo Fisher Scientific). To perform PCRs of the target genes, normalized amounts of the RT products were mixed with 12.5 μl of 2X DreamTaq™ Green PCR Master Mix (Thermo Fisher Scientific) and 1 μl of each forward and reverse primer (25 pmol/μl) to a final volume of 25 μl. PCR was performed using the standard thermal cycling conditions outlined below. The PCR products were further processed for Sanger sequencing.

The editing levels of *CYFIP2* mRNA were quantified via sequence analysis as previously described (Barbon et al., 2003) via Discovery Studio (DS) Gene 1.5 (Accelrys Inc., San Diego, CA, USA). The primers used to amplify the cDNA sequence subjected to the RNA editing process are listed in Table 1.

2.5. Cloning of human CYFIP2 variants and production of lentiviral particles

The pUC19 expression vector containing the coding sequence of human *CYFIP2* (HG16749-U) was acquired from Sino Biological, Inc., and amplified with primers containing *Age*I and *Sal*I restriction sites to insert the amplicon into pRRLSIN.cPPT.PGK-GFP.WPRE lentiviral vector (#12252 Addgene). The reverse primers also contained the sequence encoding the HA-Tag (Table 1).

To generate the edited CYFIP2 isoform (CYFIP2 E), we performed in vitro mutagenesis using a Phusion™ Site-Directed Mutagenesis Kit (Thermo Fisher Scientific) and primers bearing the desired nucleotide variation (hCYFIP2 c.958 A/G), in a PCR protocol that amplifies the entire plasmid template. The parental template was removed via the methylation-dependent endonuclease *Dpn*I (Thermo Fisher Scientific), and STBL3 bacteria were transformed with the nuclease-resistant nicked plasmid. The primers used for mutagenesis and to sequence the full inserts are displayed in Table 1.

Lentiviral particles were produced as follows: HEK293T cells were plated at low passages (no more than P8) 24 h before transfection at a density of 9.5×10^6 in 150 mm dishes; the medium was changed 2 h before transfection. The cells were cotransfected via the calcium–phosphate–DNA coprecipitation method. The plasmid mixture used was composed of 3rd-generation lentiviral plasmids, including 7 μg of the VSV-G envelope gene in the pMD2.G backbone vector (Addgene #12259), 16.25 μg of the packaging plasmid pCMV ΔR8.74 II Gen.Pack (Addgene #22036), 6.25 μg of the pRSV-rev plasmid (Addgene #12253) and 32 μg of the transfer vector (pRRLSIN.cPPT.PGK-hCYFIP2-HA.WPRE K or E (from now on pRRL-hCYFIP2-K or E) to induce the expression of CYFIP2 K or E variants or pTweenLenti-H1-shCyfip2 to downregulate the endogenous CYFIP2 protein.

The plasmid mixture was made up with a final volume of 1225 μl with Tris-EDTA 0.1 × (TE 0.1 ×)/dH2O (2:1); finally, 125 μl of CaCl2 2.5 M was added to the suspension, and the mixture was maintained for 5 min at RT. The calcium–phosphate–DNA complex was formed by adding 1250 μl of HBS 2 × solution dropwise to the mixture. The suspension was added immediately to the cells following the addition of HBS 2 × . The calcium–phosphate plasmid DNA mixture was allowed to stand on the cells for 14–16 h, after which the medium was replaced with fresh medium. After 24 h and 48 h, the medium was replaced, and the cell supernatant was collected. After ultracentrifugation at 26.000 rpm for 2 h at 4 °C, the viral pellet was subsequently resuspended in 1X PBS.

Table 1
List of primers used in the study.

Primers used for RNA editing analysis	
hCYFIP2 EF	GCCAAGAAGAGAATTAATCTTAGCAAAATTG
hCYFIP2 ER	ACTGGGGGCTGATGCTGCTCTG
Primers used to sequence the insert in pRRLSIN.cPPT.PGK-hCYFIP2-HA.WPRE vector	
hCYFIP2 352 For	GAGGTCACCAAGCTCATGAAGTTCATG
hCYFIP2 427 Rev	GCCGCTTCACCTCGCTGCAGAA
hCYFIP2 1366 For	ATGATCAAAGGCCTGCAGGTGCTC
hCYFIP2 2331 For	ATCCTTGGACCAAGCTATCAGCCG
hCYFIP2 2891 For	ATGAGTATGGCTCCCCAGGGATC
hCYFIP2 3370 For	GTGGAGTTCCACCGGCTGTGGA
hCYFIP2-436 Rev	AAAGTCCTTCCTGCGCTCGG
hCYFIP2-1450 Rev	GTCACCTGGGCGAAGTCCT
hCYFIP2-2327 For	TAAATCCTTGGACCAAGCTATCAG
hCYFIP2-2853 For	ATAGAGGTGATGCCCAAGATATGC
hCYFIP2-3516 For	TTTGACCTGTTCGACTTCTGTTACCA
Primers used to amplify the full length CDS of human CYFIP2 transcript	
hCYFIP2_AgeI_ATG_For	TTACCGGTCGCCACCATGACCACGCACGTCACCCTG
hCYFIP2_HA_TAA_SalI_Rev	ATTGTCGACTTAAGCGTAATCTGGAACATCGTATGGGTAGCAAGTGGTGGCCAAGG
Primers used to perform in vitro mutagenesis reactions	
hCYFIP2-Mut-editing-For	AGATAGAGCTGGCCAGATACATTGAGACCAGTGCTC
hCYFIP2-Mut-editing Rev	GAGCACTGGTCTCAATGTATCTGGCCAGCTCTATCT
Primers used to amplify the cyfip2 intronic region flanking the exon1, target of genome editing.	
Int-hDNA-CYFIP2-For	AGATGAAAGGTGGACGCAGCA
Int-hDNA-CYFIP2-Rev	ATGCCTCTGGTGTGAGAAGC
mCYFIP2 shRNA 3775 F	CTAGAGGCAGACCTTCAACCTGGAGGACTGCAGTCCTCCAGGTTGAAGGTCTGCTTTTTTC
mCYFIP2 shRNA 3775 R	TCGAGAAAAAAGCAGACCTTCAACCTGGAGGACTGCAGTCCTCCAGGTTGAAGGTCTGCCT

2.6. Protein extraction, quantification and Western blot

The cells harvested from primary hippocampal cultures were solubilized with modified RIPA buffer (Tris-HCl 50 mM pH 7.4, NaCl 150 mM, EDTA 1 mM, Na-DHA 0.25 %, SDS 0.1 %, NP-40 1 % and Roche protease inhibitor tablets) and then sonicated. A portion of the lysate was used for the bicinchoninic acid (BCA) protein concentration assay (Merck). Equal amounts of protein were applied to precast SDS polyacrylamide gels (4–12 % NuPAGE Bis-Tris gels; Thermo Fisher Scientific), and the proteins were electrophoretically transferred to a nitrocellulose transfer membrane (GE HealthCare) for 2 h. The membranes were blocked for 60 min with 3 % non-fat dry milk in TBS-T (Tris-buffered saline with Tween-20 0.1 %, Merck) and then incubated overnight at 4 °C in blocking solution with rabbit polyclonal anti-CYFIP1(1:500; #ab154045 Abcam), rabbit polyclonal anti-CYFIP2 (1:1000; #ab95969 Abcam), mouse monoclonal anti-GAPDH (1:10000, #MAB374 Millipore), and rabbit polyclonal anti-HA (1:1000 H6908 Merck) primary antibodies. For detection, after 3 washes in TBS-T, the membranes were incubated for 1 h at room temperature with IR-Dye secondary antibodies (1:2000 in TBS-T, LI-COR Biotech). The signals were detected via an Odyssey infrared imaging system (LI-COR Biotech) and quantified via Odyssey version 1.1 (LI-COR Biotech). The data are presented as the ratio of the intensity band of the investigated protein to that of the GAPDH band and are expressed as a percentage of the control. Each condition was carried out and analyzed in 3 independent primary culture dishes.

2.7. Indirect immunofluorescence assay

The cells were fixed with paraformaldehyde 4 % (Merck), washed three times with phosphate-buffered saline (PBS) and permeabilized with Triton X-100 0.3 % for 10 min at room temperature (RT). After 1 h of saturation with blocking solution (BSA 2 %, Triton-X-100 0.1 %, FBS 2 %), the cells were incubated for 1 h at RT with primary antibodies (rabbit polyclonal anti-CYFIP1, 1:100, #ab154045, Abcam; rabbit polyclonal anti-CYFIP2, 1:100, #ab95969, Abcam; rabbit anti-HA, 1:150, #H6908, Merck). After three washes with PBS, the cells were incubated with the secondary antibody (goat anti-rabbit Alexa Fluor™ 594, #A-11012; goat anti-rabbit Alexa Fluor™ 488, #A-11008; Thermo Fisher Scientific) at a ratio of 1:500 for 1 h at RT. The cells were washed three times with PBS, after which DAPI (Thermo Fisher Scientific) staining was performed. The coverslips were then mounted with SlowFade Gold reagent (Thermo Fisher Scientific) and observed under a fluorescence microscope.

2.8. Generation of the SH-SY5Y CYFIP2-knockout cell line

We used the CRISPR/Cas genome editing system to establish an SH-SY5Y knockout (*KO)* cell line that is deficient in both *CYFIP2* alleles (*CYFIP2*$^{-/-}$). The SH-SY5Y *CYFIP2 KO* cell line was generated by transfecting WT cells with the plasmid PX459 (pSpCas9(BB)-2A-Puro (PX459) V2.0; Addgene #62988) (Ran et al., 2013). The plasmid contains two expression cassettes: a human codon-optimized SpCas9 and a single guide RNA, which consists of 76 nt of a scaffold sequence required for Cas binding and 20 nt of a sequence that identifies the locus in the genome to be targeted. The expression of the sgRNA is under the control of the U6 promoter. After the vector was digested with *Bbs*I (#ER1011 Thermo Fisher Scientific), two annealed complementary oligos were cloned upstream of the sgRNA scaffold. The oligos were selected via the CRISPOR tool version 5.01 (http://crispor.tefor.net/) (Concordet and Haeussler, 2018), which is based on the 20 bp target sequence, followed by the 3′ end of a 3 bp NGG PAM sequence. We have chosen a prediction guide that has a high specificity score (Hsu et al., 2013) and a low number of predicted mismatches. After cloning, the Stbl3™ chemically competent *E. coli* strain (Thermo Fisher Scientific #C737303) was transformed with the purified PX459-CYFIP2-*KO* DNA plasmid.

The SH-SY5Y cell line (ATCC™, CRL2266) was transfected with the PX459-*CYFIP2-KO* DNA plasmid via Lipofectamine™ 3000 (#L3000001 Thermo Fisher Scientific) following the manufacturer's protocol. We selected transfected cells with puromycin at a concentration of 2 ng/μl for 24 h. After DNA extraction, the *CYFIP2* gene target region for Cas9 was PCR amplified and sequenced to evaluate the occurrence of genome editing events. The resulting electropherograms were assessed via the ICE analysis tool (Syntego© https://ice.synthego.com/#/).

2.9. Generation of SH-SY5Y CYFIP2 K/E knock-in cell lines

To generate a stable population of CYFIP2 K and E (SH-SY5Y knock-in (KI) cell lines), SH-SY5Y CYFIP2–KO cells were transduced with an MOI of 1 of lentiviral particles generated with the transgenic vector pRRL-hCYFIP2-K or E, as previously described, directly into the cell medium. We selected transduced cells via puromycin at a concentration of 2 ng/μl for 24 h.

2.10. Generation of a lentiviral vector to downregulate the endogenous CYFIP2 protein

shRNA-expressing vectors to downregulate the endogenous CYFIP2 protein in hippocampal cells were designed starting from the Tween-Lenti vector (7970 bp), which also contains the green fluorescent protein (GFP) coding sequence under the control of the hPGK promoter and was kindly provided by Prof. Leonardo Elia (University of Brescia). The expression of the shRNA sequence is under the control of the H1 promoter. After the vector was double digested with *Xba*I and *Xho*I (#ER0681; #ER0692 Thermo Fisher Scientific), two annealed complementary oligonucleotides carrying the palindromic sequence of the shRNA to *Cyfip2* mRNA were cloned. The sequence of the shRNA that recognizes the 3′UTR sequence of the mouse *Cyfip2* transcript starting from position 3775 was selected via the shRNA Optimal Design tool from the Kay Lab (https://med.stanford.edu/kaylab). After cloning, the Stbl3™ chemically competent *E. coli* strain (#C737303 Thermo Fisher Scientific) was transformed with pTweenLenti-H1-shCyfip2 DNA and used to generate lentiviral particles as previously described.

To generate a CYFIP2 K/E KI model, hippocampal cultures at DIV1 were transduced with a mixture of lentiviral particles containing TweenLentiH1-shCyfip2 to downregulate the endogenous CYFIP2 protein and pRRL-hCYFIP2-K or E to induce the expression of CYFIP2 K or E variants. PFA (4 %) was used to fix neuronal cultures at DIV4 or DIV17 for morphological analysis.

2.11. Confocal microscopy and imaging analysis

Fluorescently labeled cells were acquired via an inverted laser scanning confocal microscope (LSM900 Axio Observer). Z1/7 (Carl Zeiss, Jena, Germany) with an EC Plan-Neofluar 40x/1.30 Oil DIC objective, 1 slice, 625 tiles (23033x2333 pixels), Pixel Time 2.06 μs, were used for image acquisition of SH-SY5Y cells and for hippocampal cells at DIV3. For spine analysis, a Plan-Apochromat 63x/1.40 oil objective with 19 slices (6.3 μm) and a pixel time of 3.55 μs were used for image acquisition of hippocampal cells at DIV18. Pictures represent a maximum intensity projection (MIP) of 19 Z sections at 0.33 μm intervals. SH-SY5Y total neurite length, neuronal dendritic length and number of branches were measured via the plugin Simple Neurite Tracer (Arshadi et al., 2021), from Fiji image processing package (Schindelin et al., 2012). For each condition, a minimum of 15 cells were analyzed. The number of spines was measured manually via Fiji, and spine density was calculated by quantifying the number of spines in a 10 μm dendritic segment. For each condition, the spines of three secondary dendrites from a minimum of 15 cells were analyzed. Morphological analysis of SH-SY5Y cells was performed using Fiji. Following fixation with paraformaldehyde 4 %, the cytoskeleton was stained with Alexa Fluor™ 647 Phalloidin (Thermo Fisher Scientific). Fluorescently labeled cells were

imaged using an inverted laser-scanning confocal microscope. Semi-automatic segmentation of the cells in the acquired images was used to generate masks for the quantification of various morphological parameters, including cell area, F-actin signal intensity (Phalloidin intensity), and aspect ratio (major axis/minor axis) (Mariano et al., 2024). Anisotropy analysis was conducted using FibrilTool (Boudaoud et al., 2014). The anisotropy score follows this convention: 0 corresponds to no order (isotropic arrays), and 1 corresponds to perfectly ordered, parallel fibrils (anisotropic arrays).

2.12. Statistical analysis

All the cells analyzed in our study were derived from three to four independent neuronal preparations. The data are reported from single cells across cellular preparation. Data are presented as the means ± standard errors of the means (SEMs). Statistical analysis of the data was performed via GraphPad Prism 8 (GraphPad Software Inc., USA). For experiments following normal distribution, one-way ANOVA followed by Tukey's or Dunnett's post hoc test was used. For experiments that do not assume normal distribution Kruskal-Wallis test followed by Dunn's post hoc test was used. Statistical significance was assumed at $p < 0.05$.

3. Results

3.1. CYFIP2 RNA editing is conserved among organisms and modulated during neuronal maturation and by neuronal activity

To gain new insights into the functional role of *CYFIP1/2* in neuronal development, we examined their protein expression in mouse primary hippocampal neuronal cultures at different days in vitro (DIV) as a model of neuronal maturation. CYFIP1 was barely expressed at DIV4, but its expression increased throughout the differentiation process, peaking at DIV18; in contrast, CYFIP2 was highly expressed at DIV11 and stable until DIV18 (Fig. 1a). A direct comparison between CYFIP1 and CYFIP2 expression is not feasible due to the different efficacy in antibody recognition.

We then focused on CYFIP2 K/E RNA editing and aligned the protein sequences of different organisms (Fig. 1b), revealing the high conservation of amino acid residues where the editing event took place. Interestingly, *Danio rerio* and *Xenopus tropicalis* encode a CYFIP2 isoform with an E variant without RNA editing intervention. We subsequently analyzed RNA editing levels during neuronal differentiation. Our findings demonstrated that the K/E RNA editing level increased during in vitro neural development (DIV4: 15.8 %; DIV7: 24.3 %; DIV14: 36.3 %; DIV21: 61.5 %) (Fig. 1c), indicating that the process is tightly regulated

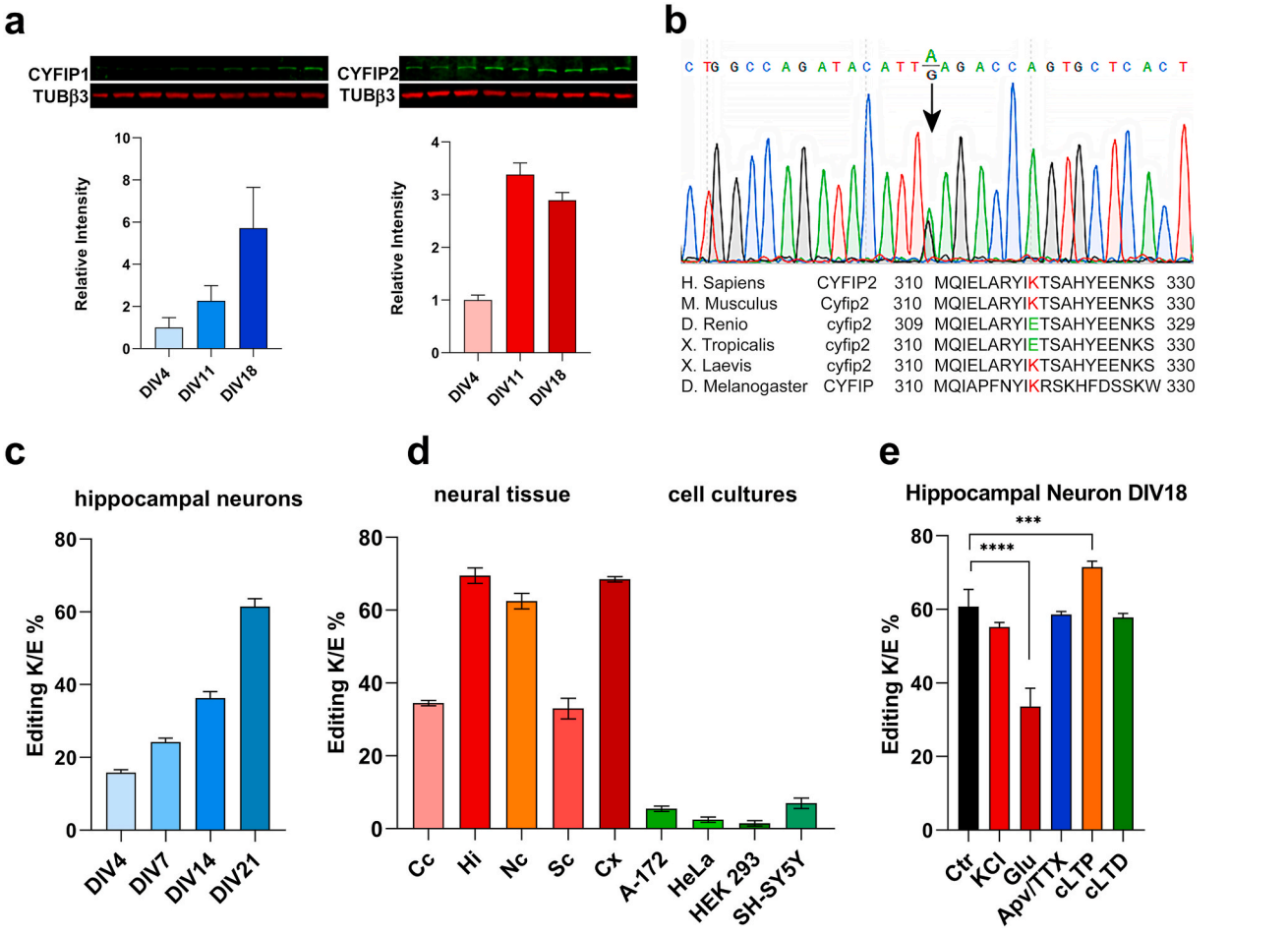

Fig. 1. (a) CYFIP1 and CYFIP2 protein expression during neuronal maturation. (b) Electropherograms from Sanger sequencing of CYFIP2 exon 10 carrying the A/I RNA editing sites. The editing site is represented by the overlapping of A and G peaks. Alignment of human CYFIP2 protein (NP_001032410.1) against the mouse (NP_598530.2), zebrafish (NP_001091056.1), Xenopus (NP_001103523.1), Drosophila (NP_650447.1) homologs showing the conservation of sequences where the edited amino acids are located. (c) Analysis of editing levels of the CYFIP2 K/E site during in vitro primary hippocampal neuron maturation, (d) in several human brain regions and cell lines, and (e) in primary hippocampal neurons after neuronal activity modulation. Statistical analysis was performed on data obtained from hippocampal neurons after neuronal activity modulation. Data are represented as mean ± SEM, n = 3–9. One-way ANOVA followed by Dunnet's multiple comparisons test $p < 0{,}005$. Data derived from at least three independent cellular preparations.

during maturation. Moreover, RNA editing levels in different human postmortem brain regions and nonneural cell line samples were examined (Fig. 1d). The editing percentages obtained from the neural tissue samples were as follows: corpus callosum (CC), 35 %; hippocampus (Hi), 71 %; caudate (Nc), 61 %; spinal cord (Sc), 31 %; and cerebral cortex (Cx), 68 %. The percentages obtained from nonneural cell lines were as follows: glioblastoma (A-172), 6 %; human cervix epithelioid carcinoma (HeLa), 2 %; human embryonic kidney (HEK293), 1 %; and human neuroblastoma (SH-SY5Y), 6 %. Our data demonstrates that the *CYFIP2* RNA editing process is specifically controlled in various brain regions and is mainly active in the central nervous system (see also Supplementary Fig. 1).

To evaluate the effects of neuronal activity on the *CYFIP2* editing process, we treated mouse primary neuronal cultures with KCl and glutamate to mimic general synaptic and glutamatergic activation and with APV/TTX to mimic synaptic blockade (Fig. 1e). Furthermore, chemical long-term potentiation (cLTP) and long-term depression (cLTD) were induced in neuronal cells. One-way ANOVA indicated a strong effect of the treatments on RNA editing levels ($F(5, 19) = 38.62$; $p < 0{,}0001$). In particular, glutamate treatment led to a decrease in the *CYFIP2* RNA editing level (Glu −44.8 %; $P < 0.0001$). The opposite effect was found after chemical LTP induction (cLTP +17.69 %, $p = 0.0005$), whereas cLTD did not induce variation.

3.1.1. *Modeling of CYFIP2 editing variants and protein–protein docking*

To evaluate the binding mode of CYFIP2 variants to the proteins forming the WAVE complex from a structural point of view, computational tools were employed. Structural data are already available in the literature for CYFIP1, as the structure of its WAVE complex was experimentally determined in the active and inactive states by means of X-ray diffraction or cryo-EM (Jumper et al., 2021; Pettersen et al., 2004). On the other hand, insights into the interaction motif of CYFIP2, particularly the K and E variants, are lacking.

Thus, in our study, we initially generated a model of the CYFIP2 K variant via AlphaFold (Jumper et al., 2021; Varadi et al., 2022), and we then produced and refined the structure of the E variant as detailed in the Materials and Methods section via UCSF Chimera 1.17.1 (Pettersen et al., 2004). Fig. 2a shows the 3D structure of the CYFIP2 K variant, and residue number 320 is highlighted in red. A detailed comparison of the residues in the K and E variants is reported in Fig. 2b.

To obtain models of the WAVE complex with CYFIP2, protein–protein docking was used. Structural studies related to autism-linked pathological variants in the WAVE regulatory complex, which are based on such techniques, have recently appeared in the literature (Xie et al., 2025). In our work, we selected the cryo-EM structures of the WAVE regulatory complex formed by CYFIP1 as templates of the active (PDB ID 7USE) and inactive (PDB ID 7USC) forms, the latter of which lacks Rac1 (Ding et al., 2022). The structures were edited by removing CYFIP1 from the models via UCSF Chimera 1.17.1 (Pettersen et al., 2004), thus obtaining "receptor" files for docking studies. The CYFIP2 K and E variants were subsequently used as "ligands" in the docking simulations, which were performed via the HDOCK server (hdock.phys.hust.edu.cn, accessed on Jan 15, 2025) (Yan et al., 2020). Thus, four models of the WAVE complex were obtained through these docking runs, namely, active WAVE/CYFIP2 K, active WAVE/CYFIP2 E, inactive WAVE/CYFIP2 K, and inactive WAVE/CYFIP2 E. These models were then ranked in terms of the docking score (-kcal/mol) and inspected via UCSF Chimera 1.17.1 (Pettersen et al., 2004).

In the case of the active WAVE complex, small differences in terms of docking scores were retrieved, as values of −621.71 kcal/mol and −621.34 kcal/mol were computed for active WAVE/CYFIP2 K and active WAVE/CYFIP2 E, respectively. Notably, in the case of the aforementioned study by Xie and colleagues, which was performed to assess the impact of pathological mutations, limited differences in terms of the affinity index were detected (Xie et al., 2025). Accordingly, from a structural point of view, CYFIP2 K and E variants share similar positions while forming their respective complexes (Fig. 2c). The residue of interest is indeed located in an exposed portion of the macromolecule, pointing toward Rac1, even if the distance between this residue and the closest residue of Rac1 (Gln2) is 8.4 Å.

In the case of the inactive complex, a docking score value of −1198.81 kcal/mol was computed for both inactive WAVE/CYFIP2 K and inactive WAVE/CYFIP2 E complexes. As evidenced by this result, no difference was obtained from this calculation in terms of the docking score. This agrees with the model depicted in Fig. 2d, where a perfect superimposition between CYFIP2 K and E variants is observed. Additionally, it must be noted that the residue of interest, in this case, is exposed to the solvent and not in proximity to other macromolecular

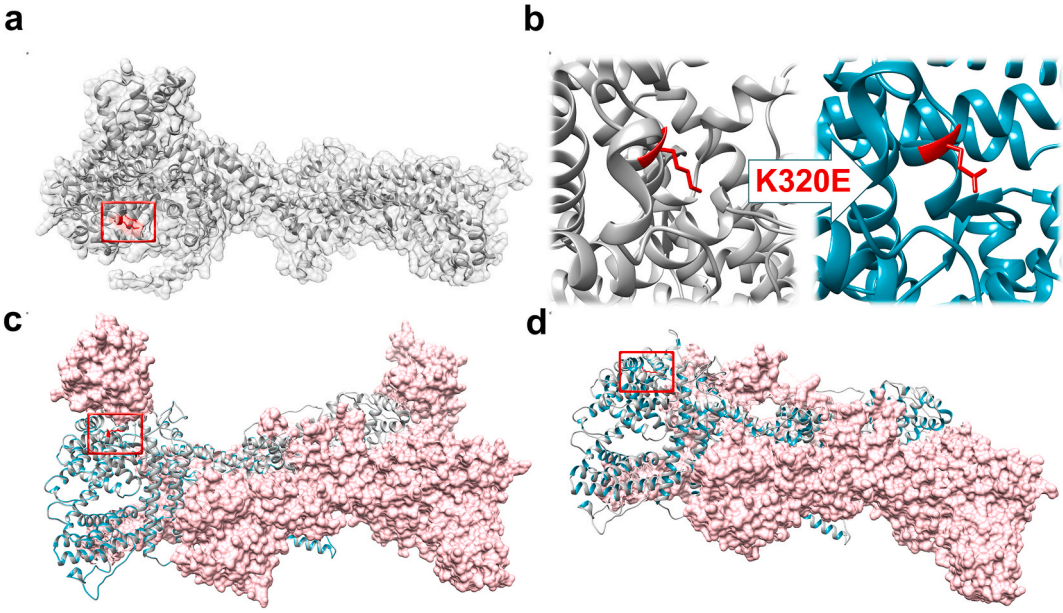

Fig. 2. (a) 3D model of CYFIP2 built with AlphaFold; (b) detailed view of the different residues presents in the CYFIP2 K and E variants. (c) 3D model of the active and (d) inactive complexes. Residues in position 320 have been highlighted in red. The CYFIP2 K structure is depicted in grey, while the E variant in sea green. The portions depicted through pink surfaces represent the parts of the macromolecules used as receptors in the docking studies.

interactions, *e.g.,* Rac1.

3.2. CYFIP2 knockout induces morphological alterations in SH-SY5Y cells that are reversed by both CYFIP2 K and E knockdown

We decided to use a neuroblastoma SH-SY5Y cell line as an in vitro model for the study of CYFIP2 K/E editing due to the ability of these cells to develop a neuronal phenotype. We established an SH-SY5Y KO cell line that is deficient in both *CYFIP2* alleles (*CYFIP2*$^{-/-}$) via CRISPR-Cas9 genome editing technology (Supplementary Fig. 2) and thus does not express the CYFIP2 protein (Fig. 3a). Furthermore, through the transduction of lentiviral particles carrying the whole CDS of the human CYFIP2 K and E isoforms, a KO cell line was used to create CYFIP2-unedited (K) and edited (E) knock-in cell lines (Fig. 3b).

The different cellular populations present remarkable differences in cell area (Kruskal-Wallis test $H_{(3)} = 179$ $p < 0{,}001$), phalloidin intensity ($H_{(3)} = 417$ $p < 0.0001$) and aspect ratio ($H_{(3)} = 44.44$ $p < 0.0001$). In particular, WT cells are characterized by a neuroblast-like phenotype with few shortened processes (Fig. 4a), whereas SH-SY5Y-CYFIP2 KO cells exhibit a striking morphological change with an increase in the cell area ($p < 0{,}0001$ vs WT) and a decrease in the aspect ratio (major axis/minor axis $p < 0{,}0001$ vs WT). Furthermore, the formation of cell blebs on the plasma membrane (Supplementary Fig. 3 and 3b) was observed. In addition, compared with WT cells, the KO cells presented completely different actin filament organization, as evidenced by the increase in stress fibers and phalloidin intensity ($p < 0{,}0001$ vs WT); notably, the overexpression of CYFIP2 K and E rescued the morphological parameters (Fig. 4b) to WT levels, and only differences in phalloidin intensity among the two CYFIP2 overexpressing cell lines were observed.

We extended our analysis with the quantification of the fiber anisotropy score, that reflects the degree of alignment or directional organization of actin filaments within the cell. One way ANOVA indicates a strong effect of the different genotypes on this score ($F(3, 158) = 39{,}13$ $p < 0{,}0001$). In particular, the anisotropy score of CYFIP2–KO was robustly reduced (−49 % vs WT, $p < 0{,}0001$), indicating a random filament orientation characteristic of a disorganized actin network. This disorganization was partially rescued by the overexpression only of the edited CYFIP2-E forms (−34 % ws WT $p < 0{,}0001$).

3.3. CYFIP2 RNA editing modulates neurite development during SH-SY5Y differentiation

Since the CYFIP2 protein is expressed mainly in neurons (Zhang et al., 2019) and the K/E RNA editing reaction is active only in the central nervous system (Levanon et al., 2005), we investigated the role of CYFIP2 K/E variants in neuronal development. For this purpose, we used a well-established model of neuronal differentiation based on the application of two-step RA and BDNF treatment to SH-SY5Y cells (Fig. 5a) (Hromadkova et al., 2020) to monitor the induction of undifferentiated SH-SY5Y cells into neuron-like cells with distinctly polarized axon−dendritic morphology. Treated cells have spindle-like morphologies with polarized appearances, with sporadic shafts and projections extending from the soma, usually one per cell. When exposed to BDNF, cellular processes expand quickly and dramatically, showing identifiable neuron-like characteristics (Fig. 5b). Kruskal-Wallis test revealed statistically significant differences in total neurite length among the groups ($H(3)$ $p < 0.0001$) (CYFIP WT mean length = 56.0 ± 3.69; CYFIP KO mean length = 15.89 ± 1.17, CYFIP-K mean length = 53.34 ± 2.89; CYFIP-E mean length = 60.04 ± 4.21). Dunn's multiple comparisons test revealed a dramatic decrease in expression after *CYFIP2* gene expression was knocked out. Furthermore, neurite development was completely restored in both *CYFIP2*-KI cell populations (K/E) (WT vs KO Mean diff. 40.14, $p < 0.0001$; KO vs K Mean diff. −37.45, $p < 0.0001$, KO vs E Mean diff. −44.15, $p < 0{,}0001$). However, no differences were detected between the CYFIP K and E cell populations (K vs E Mean diff. −6.70, $p = 0.51$), indicating that CYFIP2 is important for neuronal differentiation, but the two isoforms might have similar functions in this process in SH-SY5Y cells (Fig. 5c).

3.4. CYFIP2 RNA editing alters axon development and spine frequency in primary hippocampal neurons

Since we did not observe a clear difference in the effects of CYFIP2 K/E variants on SH-SY5Y neuronal differentiation, we used a primary neuronal culture model to understand the effects of CYFIP2 variants on neuronal maturation.

To downregulate the expression of the endogenous CYFIP2 protein, we transduced primary hippocampal neuronal cultures at DIV1 with lentiviral particles containing a shRNA targeting the 3′UTR of the *Cyfip*2 gene. Since the vector carrying the shRNA also contains the sequence coding for green fluorescent protein (GFP), we evaluated the extent of transduction via fluorescence microscopy (Fig. 6c). As shown in Fig. 6a and 48 h after transduction, the protein level of endogenous CYFIP2 was reduced by 70.2 %. CYFIP2-knockdown (CYFIP2-KD) cells were cotransduced with lentiviral particles carrying plasmids expressing the coding sequence of human CYFIP2 K or E exogenous variants to study the impact of edited or unedited CYFIP2 variants on in vitro neural maturation. Western blot analysis revealed similar expression of both exogenous CYFIP2 variants eighteen days after lentiviral transduction (Fig. 6b). The analysis of the two CYFIP2-KI lines revealed robust

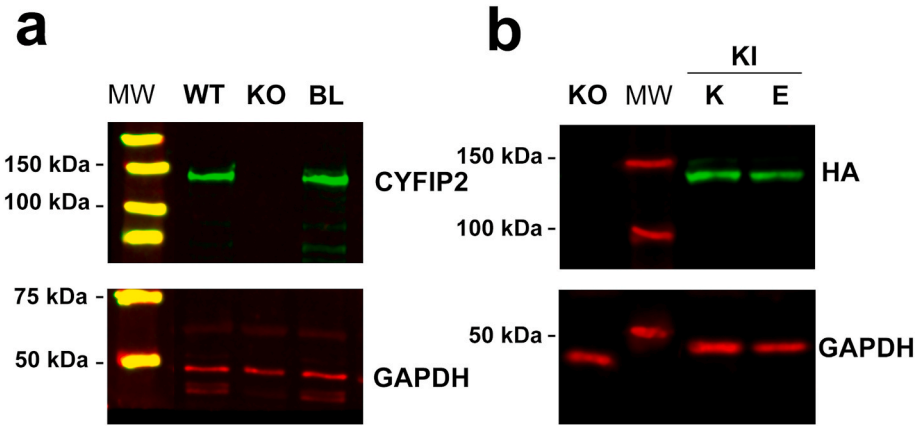

Fig. 3. (a) IR acquisition of WB obtained from cellular lysate derived from WT SHSY-5Y cell line (WT), from SHSY-5Y cell line after CRISPR/Cas9 and puromycin selection (KO) and mouse brain lysate as a positive control. Endogenous CYFIP2 proteins are detected using rabbit-α-CYFIP2 antibody. (b) IR acquisition of WB obtained from cellular lysate derived from CYFIP2 KO SHSY-5Y cell line (KO), and SHSY-5Y CYFIP2 knock-in (KI) for the K or E variants. Exogenous CYFIP2 proteins are detected using rabbit-α-HA antibody.

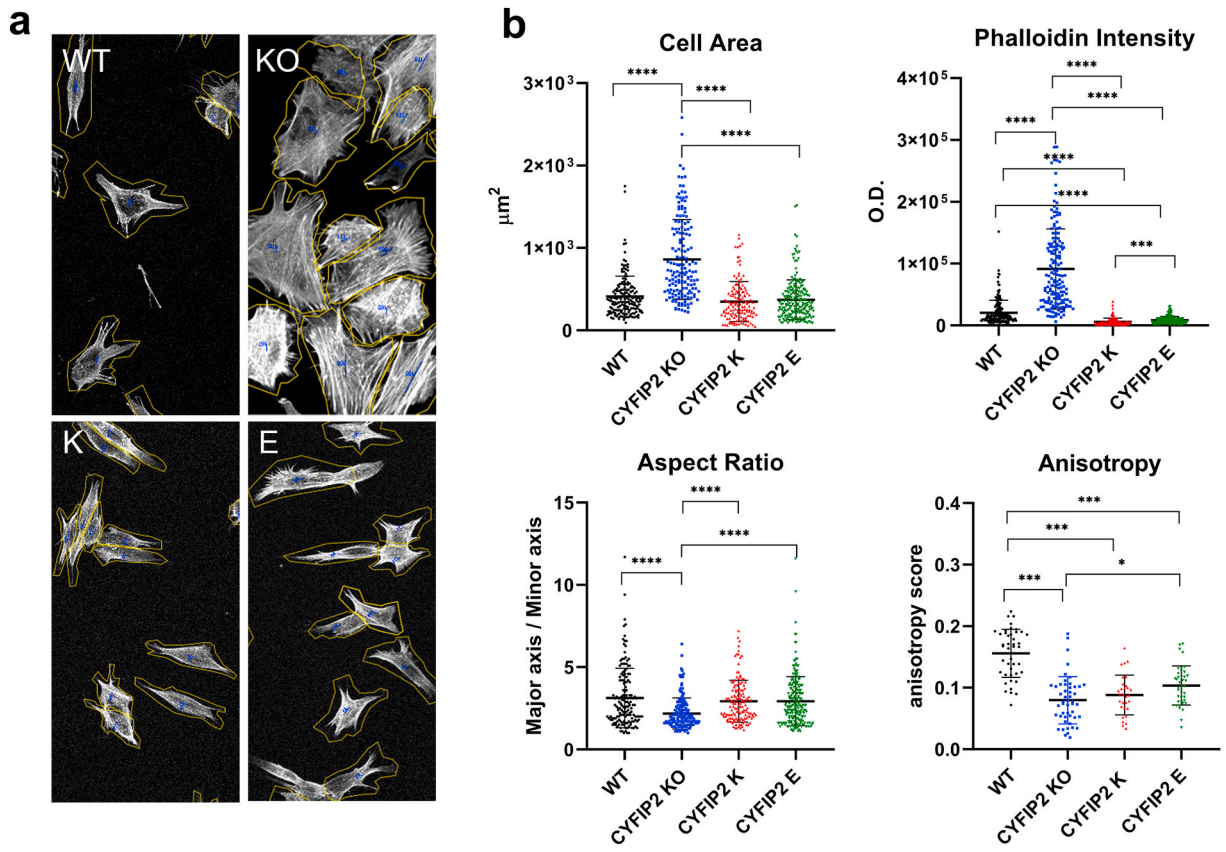

Fig. 4. (a) CYFIP2 WT, CYFIP2 KO, overexpressing CYFIP2–K and CYFIP2-E variants SH-SY5Y cells. Actin filaments are stained by phalloidin. (b) Morphological analysis of CYFIP2 WT, CYFIP2 KO, CYFIP2 K and CYFIP2 E, SH-SY5Y cell lines. The different morphological parameters (cell area, Phalloidin Intensity, Aspect Ratio: major axis/minor axis, have been analyzed with Fiji (CYFIP2 WT n = 165, CYFIP2 KO n = 161, CYFIP2 K n = 139 and CYFIP2 E n = 212). For statistical analysis Kruskal-Wallis test followed by Dunn's post hoc test was used. ***p < 0.0001, ****p < 0.0001. Anisotropy score was analyzed with the FibrilTool (CYFIP2 WT n = 44, CYFIP2 KO n = 49, CYFIP2 K n = 30 and CYFIP2 E n = 39). For statistical analysis, one-way ANOVA followed by Dunnet's multiple comparisons test p < 0,005, was used. Data are represented as mean ± SEM. Analyzed cells derived from at least three independent cultures.

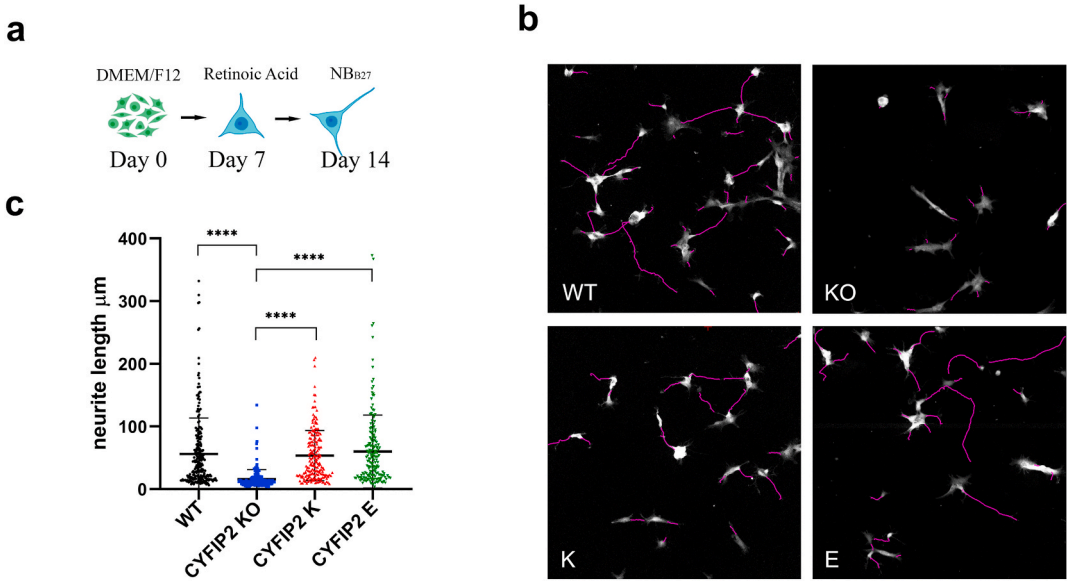

Fig. 5. (a) Schematic representation of SHSY-5Y neuronal differentiation. (b) Representative cell images for neurite length analysis by Simple Neurite Tracing. (c) Neurite length analysis of the different populations of SHSY-5Y of cells (CYFIP2 WT n = 243, CYFIP2 KO n = 173, CYFIP2 K n = 192 and CYFIP2 E n = 191. Kruskal-Wallis test followed by Dunn's post hoc test. ***p < 0.0001, ****p < 0.0001. Data are represented as mean ± SEM. Analyzed cells derived from at least three independent cultures.

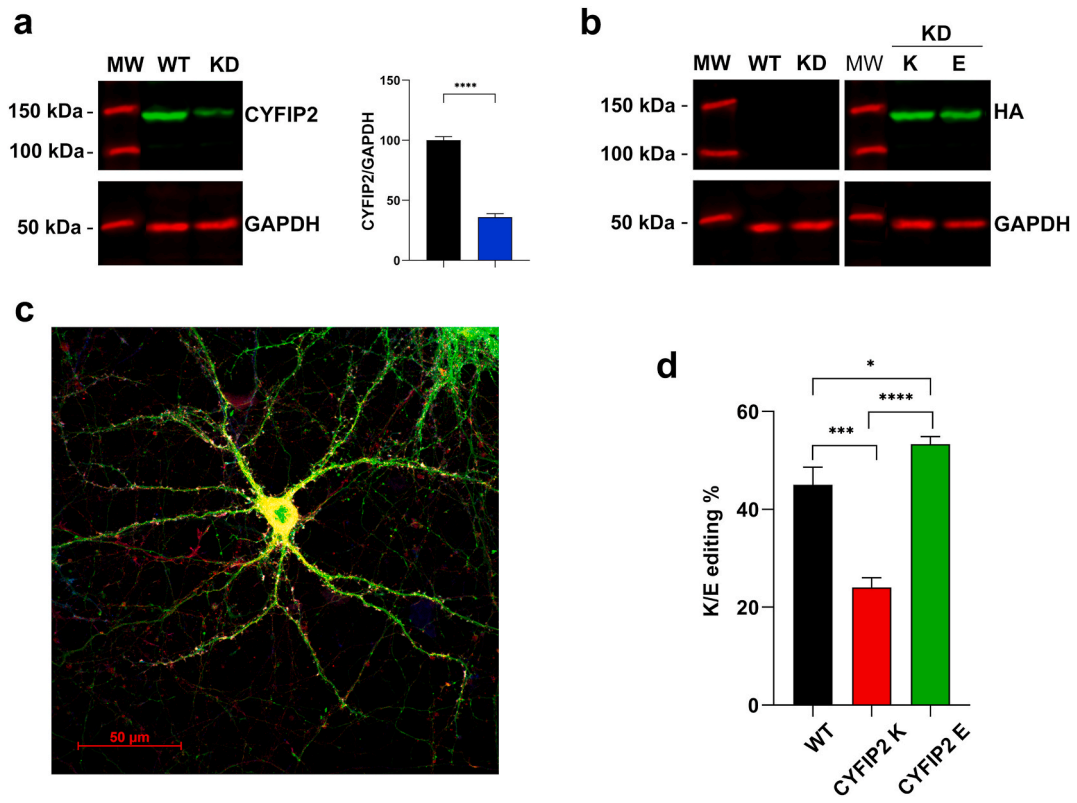

Fig. 6. (a) IR acquisition of WB obtained from cellular lysate derived from WT Hippocampal culture (WT) and after 48 from Lentiviral transduction of shRNA targeting the 3′UTR of Cyfip2 gene (KD). Endogenous CYFIP2 protein is detected with rabbit-α-CYFIP2 antibody. In the graph CYFIP2 downregulation percentage is reported. Statistical analysis was performed with student t-test. $P > 0.0001$. (b) IR acquisition of WB obtained from cellular lysate of WT, KD hippocampal cells growth for 18 DIV after lentiviral transduction with CYFIP2 K or E variants. Exogenous CYFIP2 proteins are detected using rabbit-α-HA antibody. (c) DIV18 hippocampal cell captured by confocal microscopy. The GFP protein, which represents a marker for CYFIP2 down-regulation, is detected in green. Exogenous CYFIP2 is visible in red (rabbit-α-HA antibody - goat-α-rabbit Alexa Fluor 594). (d) CYFIP2 K/E editing levels analyzed from total RNA samples obtained from wild-type hippocampal cell (WT) or CYFIP2 knock-down hippocampal cell transduced with two editing variants (CYFIP2 K; CYFIP2 E) (One way ANOVA followed by Tukey's multiple comparisons test: *$p < 0.05$ **$p < 0.01$ ***$p < 0.001$ ****$p < 0.0001$).

downregulation of the editing level of CYFIP2–K and moderate upregulation of CYFIP2-E expression relative to the control levels (One way ANOVA $F(2,6)$ $p < 0.0001$; WT = 42.0 ± 2.0 %; CYFIP2–K = 24.0 ± 1.2 %, $p < 0.001$; CYFIP2-E = 53.3 ± 1.5 %, $p < 0.05$ vs CTR; $p < 0.001$ vs K), as expected (Fig. 6d).

We initially focused on the early stages of neuronal maturation and analyzed neuronal axon length and complexity during the first days of in vitro neuronal growth (Cioni et al., 2018) (Fig. 7a). One-way ANOVA revealed a statistically significant difference among groups in each of the three parameters considered (number of branches $F(3,260)$ $p < 0.0001$; path length $F(3,260)$ $p < 0.0001$ and complexity index $F(3,260)$ $p < 0.0001$). Tukey's multiple comparisons test revealed a reduction in the number of branches (WT = 19.55 ± 1.55; CYFIP2-KD 11.13 ± 0.92 $p <$ 0,001) and path length (WT = 768.0 ± 55.1; CYFIP2-KD 427.0 ± 33.3 $p <$ 0,001) after knocking down the *CYFIP2* gene (Fig. 7b). Furthermore, the ability to produce axons with proper complexity was completely restored when KD neurons were grown overexpressing the E variant of the CYFIP2 gene but not the K variant (number of branches: CYFIP2–K: 12.45 ± 1.10; CYFIP2-E: 36.77 ± 3.49; path length: CYFIP2–K: 658.6 ± 59.4; CYFIP2-E: 1141 ± 99.6). The complexity of the axons in neurons carrying the CYFIP2 E variant was significantly greater than that in WT neurons (Fig. 7b).

Actin dynamics are essential for synaptic function, spine formation, and plasticity (Citri and Malenka, 2008). The frequency of the spines, which is the number of spines every 10 µm in the length of the secondary dendrite (Fig. 8a), significantly changed among the three different experimental groups (Fig. 8b: one-way ANOVA $F(3,69)$ $p < 0,0001$). In particular, compared with WT cells, CYFIP2-KD cells presented a decreased spine frequency (WT: 3.65 ± 0.23; CYFIP2-KD: 2.06 ± 0.16; Tukey's multiple comparisons test, WT vs. KD; $p < 0.0001$). This decrease remained similar when the expression of the K variant was induced (CYFIP2 K: 2.50 ± 0.12; WT vs. K $p < 0.0001$), indicating that the physiological frequency of spines did not recover after the expression of the CYFIP2 K variant (CYFIP2 KD vs. K ns $p < 0.3832$). In contrast, this parameter was completely restored after the expression of the CYFIP2 E variant (CYFIP2 E: 3.82 ± 0.26; KD vs. E $p < 0.0001$). This difference was also statistically significant between the K and E groups (CYFIP2 K vs. E $p < 0.0001$). Taken together, these results suggest a clear role for the CYFIP2 K/E RNA editing process in regulating spinogenesis in hippocampal neurons in vitro.

4. Discussion

CYFIP2 is one of the few neuro-specific transcripts that undergo RNA editing (Levanon et al., 2005) in the coding sequence, resulting in a K/E substitution at amino acid 320; nevertheless, its functional meaning is still unknown. Here, we provide evidence that CYFIP2 K/E editing plays a role in neuronal axon and spine maturation, at least in primary neurons.

CYFIP2 editing is mediated by ADAR2, which is especially abundant in the cortex and cerebellar tissues (Nishimoto et al., 2008; Riedmann et al., 2008). A-to-I editing by ADARs also plays a role in embryogenesis and aging, especially in the brain, highlighting its importance throughout the lifetime. In mice, the RNA editing level of ADAR targets, including *CYFIP2*, increases throughout embryo development, and in some cases, it reaches almost 90 % after 21 postnatal days (Dillman

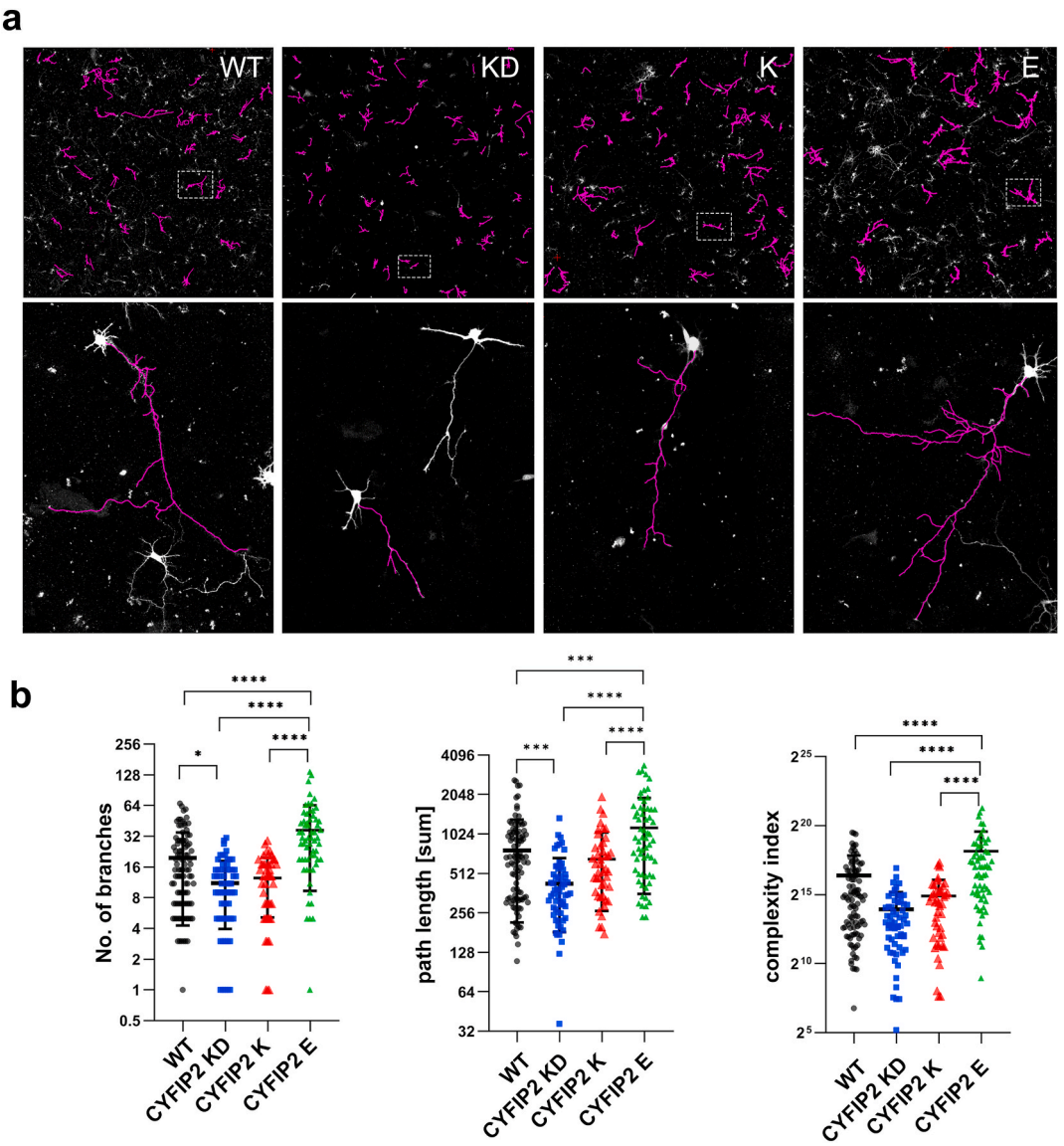

Fig. 7. (a) Axon length analysis of hippocampal culture at DIV4 by Simple Neurite Tracing is shown in purple. (b) The complexity of axonal arborization was determined by analysing the number of branches, the total length of axons and the complexity index. (N = 97 (WT), 61 (KD), 44 (CYFIP2 K), 62 (CYFIP2 E); for statistical analysis, one way ANOVA followed by Tukey's multiple comparisons test was used: *p < 0.05; **p < 0.01 ***p < 0.001; ****p < 0.0001.

et al., 2013; Nishimoto et al., 2008). Recently, it was shown that the level of *CYFIP2* RNA editing is high only in neurons, together with a high level of protein expression (Levitsky et al., 2019). *CYFIP2* RNA editing is undetectable in human embryonic stem cells and fetal brains, whereas its level increases in the adult brain (Shtrichman et al., 2012). Interestingly, an age-dependent decrease in *CYFIP2* editing has been reported in the adult human brain (Nicholas et al., 2010). Additionally, we previously demonstrated that rat cortical cells treated with glutamate, the main excitatory neurotransmitter, presented decreased *CYFIP2* RNA editing levels in parallel with the downregulation of ADAR2 expression and self-editing (Bonini et al., 2015), indicating a role of this editing site in modulation of excitatory neurotransmission. Recently, modifications in *CYFIP2* editing levels have been linked to chronic social conflict (Ru et al., 2022).

The results reported here show that the *CYFIP2* RNA editing reaction increases during neural development in a manner similar to that of other edited neuro-specific transcripts (Orlandi et al., 2011) and that it is specifically regulated in different brain areas, suggesting a role during neuronal development and function. Furthermore, the level of CYFIP2 RNA editing in hippocampal cultures varied under synaptic modulation, suggesting that CYFIP2 editing might act as an activity-dependent molecular switch modulating dendritic spine morphology and synaptic strength. In particular a robust downregulation was observed after chronic glutamate treatment, somehow representing a compensatory response set in motion by neuronal cells in order to attenuate, at least partially, glutamate excitotoxicity, as already reported in cortical neurons (Bonini et al., 2015). Of note, chemical LTP induces slight increase of CYFIP2 editing level, indicating that the up-regulation of this epitrascriptomic process might be implicated in the potentiation of excitatory synapsis. In this line, aberrant editing of CYFIP2 during critical developmental windows could impair synaptic connectivity and contribute to neurodevelopmental disorders such as autism, epilepsy, or intellectual disability (Zhang et al., 2019). Given CYFIP2's role in actin cytoskeleton remodeling and synaptic plasticity through its interaction with the WAVE regulatory complex and in FMRP dependent protein synthesis (Zhang et al., 2019), activity-dependent editing could fine-tune its function in response to neuronal stimulation. Future studies should address how RNA editing affects CYFIP2 protein interactions and downstream cytoskeletal dynamics, and whether targeted manipulation of RNA editing can restore proper neuronal function in disease models.

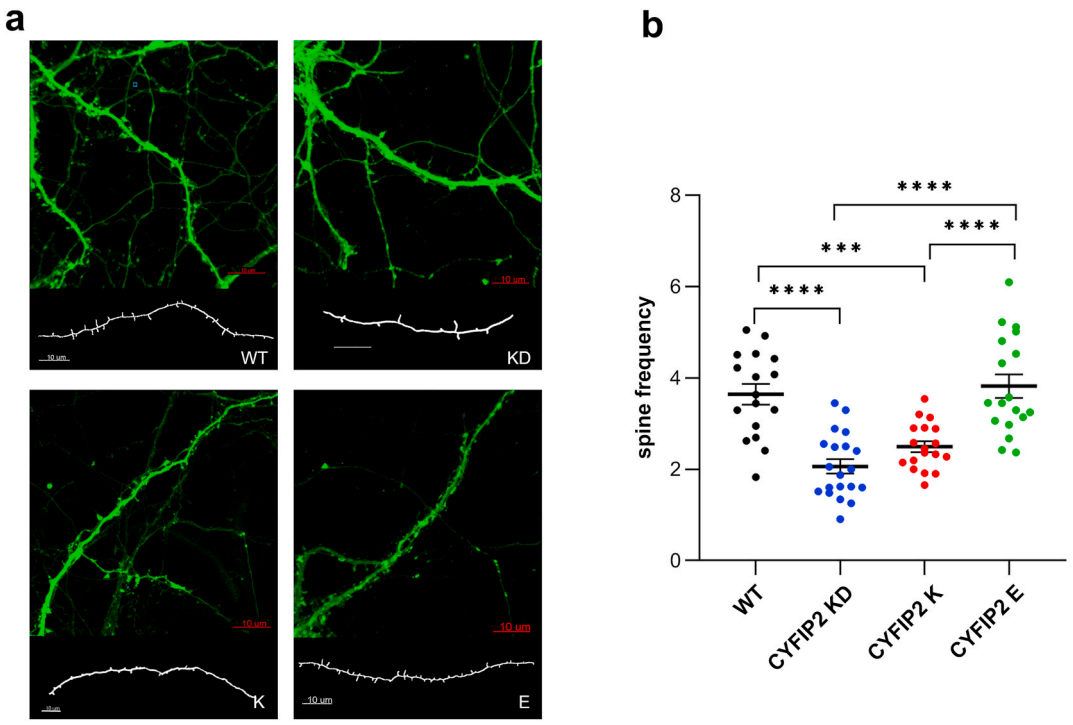

Fig. 8. (a) Image of secondary dendrite hippocampal neurons at DIV18, captured by confocal microscopy. GFP protein signal visible in green, represents a marker of CYFIP2 down-regulation. In white, the reconstruction of dendrites and spine structures by imageJ is reported. (b) Distribution of spine frequency of the different populations of CYFIP2 cells (right) (N = 17 (WT), 20 (KD), 18 (CYFIP2 K), 18 (CYFIP2 E); for statistical analysis, one way ANOVA followed by Tukey's multiple comparisons test was used: ***<0.001 ****<0.0001.

The CYFIP2 protein is a fundamental component of the wave regulatory complex (WRC), a key hub for signaling between the plasma membrane and actin dynamics involved in a variety of functions. In its basal state, the WRC is inactive in the cytosol. After various upstream signals arise from growth factors, WRCs can be recruited to specific membrane regions where they activate the Arp2/3 complex to promote actin polymerization (Bonini et al., 2015; Ru et al., 2022). The interaction of Rac1 with the WRC is the primary driver of complex activation. The active form of Rac (Rac-GTP) binds to the two sites of WRC (A and D) present in the CYFIP2 structure (or CYFIP1) and drives a series of conformational changes in the WRC structure that lead to the release of the VCA domain, which is free to activate the Arp2/3 complex to promote actin polymerization (Schaks et al., 2018).

Accordingly, in our predicted 3D models, we observed that residue 320 is indeed located in an exposed portion of CYFIP2, pointing toward Rac1. Even if the measured distance is not sufficient to justify its involvement in a strong binding interaction, the variation of the residue from K to E leads to a small difference in terms of the calculated binding energy, which can be appreciated only if Rac1 is present and was not observed for the model of the inactive form.

To investigate whether CYFIP2 K/E RNA editing regulation can be implicated in the control of actin dynamics, we initially used CYFIP2 KO neuroblastoma cell lines as an in vitro model. Compared with WT cells, SH-SY5Y cells lost their characteristic neuroblast-like phenotype after CYFIP2 gene knockdown, exhibiting a striking morphological change, with the formation of cell blebs on the plasma membrane and completely different actin filament organization. To confirm the role of the CYFIP2 protein in actin cytoskeleton organization, we generated two stable SH-SY5Y CYFIP2 KI cell lines, one expressing the unedited CYFIP2 K variant and one expressing the edited CYFIP2 E variant. As expected, CYFIP2 KO showed severe cytoskeletal disorganization, with increased cell areas and stress fiber formation. These alterations were mainly reverted when both CYFIP2 K/E variants were overexpressed, with CYFIP2-E showing the higher rescue capability. However, while these data highlight the role of CYFIP2 in actin dynamics, they do not clearly indicate a distinct effect of the edited variants.

Since the CYFIP2 protein is expressed mainly in neurons (Zhang et al., 2019) and the K/E RNA editing reaction is active only in the central nervous system, we investigated the role of CYFIP2 K/E variants in neuronal development. For this purpose, we used a model of neuronal differentiation based on the application of RA and BDNF factor (Hromadkova et al., 2020) to SH-SY5Y cells to monitor the conversion of undifferentiated cells into neuron-like cells. Differentiated WT cells assume a characteristic neuron-like morphology, but in contrast, CYFIP2 KO cells display a distinctive fibroblast-like morphology with a non-polarized appearance and large soma. This evidence, which suggests the involvement of the CYFIP2 protein in the process of neuronal development, was confirmed when we differentiated the CYFIP2-KI cell lines. We observed complete restoration of neurite development in both CYFIP2-KI cell populations (K/E). However, a clearly distinct function of the edited isoforms could not be described.

CYFIP2 has been shown to be involved in the growth and sorting of retinal ganglion cell axons (Cioni et al., 2018). For this reason, we initially focused on the early stages of neuronal maturation and used mouse hippocampal neurons to analyze axon length and complexity during the first days of in vitro neuronal development. Hippocampal neurons were co-transduced with lentiviral particles expressing CYFIP2 K or E variants together with lentivirus expressing shRNA to down-regulate the endogenous CYFIP2 protein to assess the impact of RNA editing alterations, excluding the effects of endogenous proteins. Increasing the expression of the unedited CYFIP2 variant (K) leads to a simplification of axon development in terms of the number of branches and axonal length, which is quite similar to the KD of CYFIP2. Conversely, an increase in the expression of the edited variant (E) results in an increase in axon complexity, even in comparison to WT neurons. Furthermore, we measured the frequency of spines in the secondary dendrites of mature neurons. Compared with WT cells, CYFIP2-silenced cells presented a decreased spine frequency. This decrease was similar

when we induced the expression of the K variant in the cells, indicating that the physiological frequency of spines did not recover after the expression of the CYFIP2 K variant. Conversely, this parameter was completely restored after the expression of the CYFIP2 E variant. Taken together, these results suggest a clear role of the CYFIP2 K/E RNA editing process in regulating both the outgrowth of neuronal axons during the first stages of in vitro development and the process of spinogenesis in the subsequent stages of in vitro development in hippocampal cells. In both processes, the branching of β-actin fibers seems to be essential. However, our data do not directly link CYFIP2 RNA editing with actin polymerization. Additional experiments that specifically assess actin polymerization or related signaling pathways would provide more evidence. Though, these experiments might be challenging in a mixed neuronal cellular population such as that reported here and different experimental models should be used. Furthermore, CYFIP2, together with its paralog CYFIP1, was originally identified as a binding partner of the Fragile X Mental Retardation Protein (FMRP) (Schenck et al., 2001). Through this interaction, CYFIP proteins participate in a translational repression complex with FMRP and eIF4E, regulating activity-dependent local protein synthesis at synapses (Napoli et al., 2008). Synaptic stimulation, for example by BDNF or mGluR activation, can lead to the dissociation of CYFIP from eIF4E and the subsequent release of translational repression, allowing for activity-dependent local protein synthesis (Napoli et al., 2008). Recent studies further show that CYFIP2–FMRP interactions are critical for synaptic development, behavior, and neurodevelopmental disorders (Han et al., 2015). Cyfip2 haploinsufficient mice display abnormal dendritic spine morphology and impaired synaptic plasticity (Han et al., 2015; Kang et al., 2023; Ma et al., 2025). Furthermore, in zebrafish, mutations in cyfip2 that disrupt its interaction with FMRP result in abnormal acoustic startle behavior, confirming the in vivo functional significance of this molecular interaction (Deslauriers et al., 2024; Marsden et al., 2018). Consistent with these experimental findings, human genetic studies have linked de novo mutations in CYFIP2 to intellectual disability and seizures, with several variants predicted to alter CYFIP2's protein–protein interactions, including those relevant to FMRP function (Zweier et al., 2019). Together, these studies highlight CYFIP2 as a critical FMRP partner involved in the regulation of local translation, synaptic development, and neurodevelopmental disease. We cannot exclude that the axon and spine morphological alterations reported in the present manuscript might be due, at least in part, to alteration in FMRP dependent local protein synthesis of important synaptic mRNAs. Future studies will be needed at dissecting these mechanisms in greater depth.

In conclusion, the epi-transcriptomic A-to-I RNA editing can be temporally modulated to accurately modify the functions of neuronal genes throughout brain development. Thus, numerous layers of control are necessary to build a sophisticated organ system such as the brain. An increasing amount of evidence supports this idea, showing that RNA editing plays a crucial role in the regulation of central nervous system physiology (Behm and Öhman, 2016). During the process of neural differentiation and maturation and in all stages of brain development, from the embryo stage to the development of adult tissues, the level of RNA editing of important neurospecific transcripts dynamically changes (Behm and Öhman, 2016; Cioni et al., 2018). Our research reveals for the first time how actin dynamic processes are related to the CYFIP2 K/E RNA editing process in neuronal development and function. Further studies are necessary to determine whether this process is equally relevant in vivo.

CRediT authorship contribution statement

Luca La Via: Writing – review & editing, Writing – original draft, Formal analysis, Data curation, Conceptualization. **Elona Ndoj:** Data curation. **Matteo Bertoli:** Investigation, Data curation. **Veronica Mutti:** Investigation, Formal analysis, Data curation. **Giulia Carini:** Investigation, Formal analysis, Data curation. **Alice Filippini:** Investigation, Formal analysis, Data curation. **Federica Bono:** Investigation, Formal analysis, Data curation. **Chiara Fiorentini:** Writing – review & editing, Formal analysis. **Giovanni Ribaudo:** Investigation, Formal analysis, Data curation. **Alessandra Gianoncelli:** Investigation, Formal analysis, Data curation. **Giuseppe Borsani:** Writing – review & editing, Formal analysis. **Isabella Russo:** Writing – review & editing, Formal analysis. **Alessandro Barbon:** Writing – review & editing, Writing – original draft, Conceptualization.

Ethics approval

This study was performed in line with the principles of the Declaration of Helsinki. Approval was granted by the Ethics Committee of University of Brescia (Project ID: 211B5.N.TMW).

Funding

This research did not receive any specific grant from funding agencies in the public, commercial, or not-for-profit sectors.

Declaration of competing interest

The authors declare that they have no known competing financial interests or personal relationships that could have appeared to influence the work reported in this paper.

Acknowledgments

The authors performed experiments at the Imaging Platform of the Department of Molecular and Translational Medicine at the university of Brescia.

Appendix A. Supplementary data

Supplementary data to this article can be found online at https://doi.org/10.1016/j.neuint.2025.106084.

References

Arshadi, C., Günther, U., Eddison, M., Harrington, K.I.S., Ferreira, T.A., 2021. SNT: a unifying toolbox for quantification of neuronal anatomy. Nat. Methods 18 (4), 374–377. https://doi.org/10.1038/s41592-021-01105-7.

Barbon, A., Vallini, I., La Via, L., Marchina, E., Barlati, S., 2003. Glutamate receptor RNA editing: a molecular analysis of GluR2, GluR5 and GluR6 in human brain tissues and in NT2 cells following in vitro neural differentiation. Brain Res. Mole. Brain Res. 117 (2), 168–178. https://doi.org/10.1016/s0169-328x(03)00317-6.

Behm, M., Öhman, M., 2016. RNA editing: a contributor to neuronal dynamics in the Mammalian brain. Trends Genet.: TIG (Trends Genet.) 32 (3), 165–175. https://doi.org/10.1016/j.tig.2015.12.005.

Bonini, D., Filippini, A., La Via, L., Fiorentini, C., Fumagalli, F., Colombi, M., Barbon, A., 2015. Chronic glutamate treatment selectively modulates AMPA RNA editing and ADAR expression and activity in primary cortical neurons. RNA Biol. 12 (1), 43–53. https://doi.org/10.1080/15476286.2015.1008365.

Boudaoud, A., Burian, A., Borowska-Wykręt, D., Uyttewaal, M., Wrzalik, R., Kwiatkowska, D., Hamant, O., 2014. FibrilTool, an ImageJ plug-in to quantify fibrillar structures in raw microscopy images. Nat. Protoc. 9 (2), 457–463. https://doi.org/10.1038/nprot.2014.024.

Chen, Z., Borek, D., Padrick, S.B., Gomez, T.S., Metlagel, Z., Ismail, A.M., Umetani, J., Billadeau, D.D., Otwinowski, Z., Rosen, M.K., 2010. Structure and control of the actin regulatory WAVE complex. Nature 468 (7323), 533–538. https://doi.org/10.1038/nature09623.

Cioni, J.-M., Wong, H.H.-W., Bressan, D., Kodama, L., Harris, W.A., Holt, C.E., 2018. Axon-Axon interactions regulate topographic optic tract sorting via CYFIP2-Dependent WAVE complex function. Neuron 97 (5), 1078–1093.e6. https://doi.org/10.1016/j.neuron.2018.01.027.

Citri, A., Malenka, R.C., 2008. Synaptic plasticity: multiple forms, functions, and mechanisms. Neuropsychopharmacology: Off. Public. Am. College Neuropsychopharmacol. 33 (1). https://doi.org/10.1038/sj.npp.1301559. Article 1.

Concordet, J.-P., Haeussler, M., 2018. CRISPOR: intuitive guide selection for CRISPR/Cas9 genome editing experiments and screens. Nucleic Acids Res. 46 (W1), W242–W245. https://doi.org/10.1093/nar/gky354.

Deslauriers, J.C., Ghotkar, R.P., Russ, L.A., Jarman, J.A., Martin, R.M., Tippett, R.G., Sumathipala, S.H., Burton, D.F., Cole, D.C., Marsden, K.C., 2024. Cyfip2 controls the acoustic startle threshold through FMRP, actin polymerization, and GABAB receptor

function. bioRxiv: Preprint Server Biol. 12 (22), 573054. https://doi.org/10.1101/2023.12.22.573054, 2023.
Dillman, A.A., Hauser, D.N., Gibbs, J.R., Nalls, M.A., McCoy, M.K., Rudenko, I.N., Galter, D., Cookson, M.R., 2013. mRNA expression, splicing and editing in the embryonic and adult mouse cerebral cortex. Nat. Neurosci. 16 (4), 499–506. https://doi.org/10.1038/nn.3332.
Ding, B., Yang, S., Schaks, M., Liu, Y., Brown, A.J., Rottner, K., Chowdhury, S., Chen, B., 2022. Structures reveal a key mechanism of WAVE regulatory complex activation by Rac1 GTPase. Nat. Commun. 13 (1), 5444. https://doi.org/10.1038/s41467-022-33174-3.
Han, K., Chen, H., Gennarino, V.A., Richman, R., Lu, H.-C., Zoghbi, H.Y., 2015. Fragile X-like behaviors and abnormal cortical dendritic spines in cytoplasmic FMR1-interacting protein 2-mutant mice. Hum. Mol. Genet. 24 (7), 1813–1823. https://doi.org/10.1093/hmg/ddu595.
Hromadkova, L., Bezdekova, D., Pala, J., Schedin-Weiss, S., Tjernberg, L.O., Hoschl, C., Ovsepian, S.V., 2020. Brain-derived neurotrophic factor (BDNF) promotes molecular polarization and differentiation of immature neuroblastoma cells into definitive neurons. Biochim. Biophys. Acta Mol. Cell Res. 1867 (9), 118737. https://doi.org/10.1016/j.bbamcr.2020.118737.
Hsu, P.D., Scott, D.A., Weinstein, J.A., Ran, F.A., Konermann, S., Agarwala, V., Li, Y., Fine, E.J., Wu, X., Shalem, O., Cradick, T.J., Marraffini, L.A., Bao, G., Zhang, F., 2013. DNA targeting specificity of RNA-guided Cas9 nucleases. Nat. Biotechnol. 31 (9), 827–832. https://doi.org/10.1038/nbt.2647.
Jumper, J., Evans, R., Pritzel, A., Green, T., Figurnov, M., Ronneberger, O., Tunyasuvunakool, K., Bates, R., Žídek, A., Potapenko, A., Bridgland, A., Meyer, C., Kohl, S.A.A., Ballard, A.J., Cowie, A., Romera-Paredes, B., Nikolov, S., Jain, R., Adler, J., et al., 2021. Highly accurate protein structure prediction with AlphaFold. Nature 596 (7873), 583–589. https://doi.org/10.1038/s41586-021-03819-2.
Kang, M., Zhang, Y., Kang, H.R., Kim, S., Ma, R., Yi, Y., Lee, S., Kim, Y., Li, H., Jin, C., Lee, D., Kim, E., Han, K., 2023. P.Arg87Cys causes neurological defects and degradation of CYFIP2. Ann. Neurol. 93 (1), 155–163. https://doi.org/10.1002/ana.26535.
Konietzny, A., Bär, J., Mikhaylova, M., 2017. Dendritic actin Cytoskeleton: structure, functions, and regulations. Front. Cell. Neurosci. 11. https://doi.org/10.3389/fncel.2017.00147.
Levanon, E.Y., Hallegger, M., Kinar, Y., Shemesh, R., Djinovic-Carugo, K., Rechavi, G., Jantsch, M.F., Eisenberg, E., 2005. Evolutionarily conserved human targets of adenosine to inosine RNA editing. Nucleic Acids Res. 33 (4), 1162–1168. https://doi.org/10.1093/nar/gki239.
Levitsky, L.I., Kliuchnikova, A.A., Kuznetsova, K.G., Karpov, D.S., Ivanov, M.V., Pyatnitskiy, M.A., Kalinina, O.V., Gorshkov, M.V., Moshkovskii, S.A., 2019. Adenosine-to-Inosine RNA editing in mouse and human brain proteomes. Proteomics 19 (23), e1900195. https://doi.org/10.1002/pmic.201900195.
Ma, R., Kang, M., Kim, G.H., Kang, H., Lee, S., Yang, Y., Lee, H.J., Choi, S., Kim, S., Kim, S., Jun, Y., Kim, H., Zhang, Y., Kim, U.S., Kang, H.R., Kim, Y., Lee, Y., Chung, W., Lee, E.J., et al., 2025a. Seizure evolution in a mouse model of West syndrome involves complex and time-dependent synapse remodeling, gliosis and alterations in lipid metabolism. PLoS Biol. 23 (10), e3003192. https://doi.org/10.1371/journal.pbio.3003192.
Ma, R., Kim, U.S., Chung, Y., Kang, H.R., Zhang, Y., Han, K., 2025b. Recent advances in CYFIP2-associated neurodevelopmental disorders: from human genetics to molecular mechanisms and mouse models. Brain Dev. 47 (1). https://doi.org/10.1016/j.braindev.2024.104302.
Mariano, V., Kanellopoulos, A.K., Ricci, C., Di Marino, D., Borrie, S.C., Dupraz, S., Bradke, F., Achsel, T., Legius, E., Odent, S., Billuart, P., Bienvenu, T., Bagni, C., 2024. Intellectual disability and behavioral deficits linked to *CYFIP1* missense variants disrupting actin polymerization. Biol. Psychiatry 95 (2), 161–174. https://doi.org/10.1016/j.biopsych.2023.08.027.
Marsden, K.C., Jain, R.A., Wolman, M.A., Echeverry, F.A., Nelson, J.C., Hayer, K.E., Miltenberg, B., Pereda, A.E., Granato, M., 2018. A Cyfip2-Dependent excitatory interneuron pathway establishes the innate startle threshold. Cell Rep. 23 (3), 878–887. https://doi.org/10.1016/j.celrep.2018.03.095.
Mingardi, J., La Via, L., Tornese, P., Carini, G., Trontti, K., Seguini, M., Tardito, D., Bono, F., Fiorentini, C., Elia, L., Hovatta, I., Popoli, M., Musazzi, L., Barbon, A., 2021. miR-9-5p is involved in the rescue of stress-dependent dendritic shortening of hippocampal pyramidal neurons induced by acute antidepressant treatment with ketamine. Neurobiol. Stress 15, 100381. https://doi.org/10.1016/j.ynstr.2021.100381.
Napoli, I., Mercaldo, V., Boyl, P.P., Eleuteri, B., Zalfa, F., De Rubeis, S., Di Marino, D., Mohr, E., Massimi, M., Falconi, M., Witke, W., Costa-Mattioli, M., Sonenberg, N., Achsel, T., Bagni, C., 2008. The fragile X syndrome protein represses activity-dependent translation through CYFIP1, a new 4E-BP. Cell 134 (6), 1042–1054. https://doi.org/10.1016/j.cell.2008.07.031.
Nicholas, A., de Magalhaes, J.P., Kraytsberg, Y., Richfield, E.K., Levanon, E.Y., Khrapko, K., 2010. Age-related gene-specific changes of A-to-I mRNA editing in the human brain. Mech. Ageing Dev. 131 (6), 445–447. https://doi.org/10.1016/j.mad.2010.06.001.
Nishimoto, Y., Yamashita, T., Hideyama, T., Tsuji, S., Suzuki, N., Kwak, S., 2008. Determination of editors at the novel A-to-I editing positions. Neurosci. Res. 61 (2), 201–206. https://doi.org/10.1016/j.neures.2008.02.009.
Omotade, O.F., Pollitt, S.L., Zheng, J.Q., 2017. Actin-based growth cone motility and guidance. Mol. Cell. Neurosci. 84, 4–10. https://doi.org/10.1016/j.mcn.2017.03.001.
Orlandi, C., Barbon, A., Barlati, S., 2012. Activity regulation of adenosine deaminases acting on RNA (ADARs). Mol. Neurobiol. 45 (1), 61–75. https://doi.org/10.1007/s12035-011-8220-2.
Orlandi, C., La Via, L., Bonini, D., Mora, C., Russo, I., Barbon, A., Barlati, S., 2011. AMPA receptor regulation at the mRNA and protein level in rat primary cortical cultures. PLoS One 6 (9), e25350. https://doi.org/10.1371/journal.pone.0025350.
Otmakhov, N., Khibnik, L., Otmakhova, N., Carpenter, S., Riahi, S., Asrican, B., Lisman, J., 2004. Forskolin-induced LTP in the CA1 hippocampal region is NMDA receptor dependent. J. Neurophysiol. 91 (5), 1955–1962. https://doi.org/10.1152/jn.00941.2003.
Pettersen, E.F., Goddard, T.D., Huang, C.C., Couch, G.S., Greenblatt, D.M., Meng, E.C., Ferrin, T.E., 2004. UCSF Chimera—A visualization system for exploratory research and analysis. J. Comput. Chem. 25 (13), 1605–1612. https://doi.org/10.1002/jcc.20084.
Pollard, T.D., 2016. Actin and actin-binding proteins. Cold Spring Harbor Perspect. Biol. 8 (8). https://doi.org/10.1101/cshperspect.a018226. Article 8.
Ran, F.A., Hsu, P.D., Wright, J., Agarwala, V., Scott, D.A., Zhang, F., 2013. Genome engineering using the CRISPR-Cas9 system. Nat. Protoc. 8 (11), 2281–2308. https://doi.org/10.1038/nprot.2013.143.
Riedmann, E.M., Schopoff, S., Hartner, J.C., Jantsch, M.F., 2008. Specificity of ADAR-Mediated RNA editing in newly identified targets. RNA (New York, N.Y.) 14 (6), 1110–1118. https://doi.org/10.1261/rna.923308.
Ru, F.-X., Kong, F., Ren, C.-Y., He, Y.-S., Xia, S.-Y., Li, Y.-N., Liang, Y.-P., Feng, J.-J., Wei, Z.-Y., Chen, J.-H., 2022. Repeated winning and losing experiences in chronic social conflicts are linked to RNA editing pattern difference. Front. Psychiatr. 13, 896794. https://doi.org/10.3389/fpsyt.2022.896794.
Schaks, M., Singh, S.P., Kage, F., Thomason, P., Klünemann, T., Steffen, A., Blankenfeldt, W., Stradal, T.E., Insall, R.H., Rottner, K., 2018. Distinct interaction sites of rac GTPase with WAVE regulatory complex have non-redundant functions in vivo. Curr. Biol.: CB 28 (22), 3674–3684.e6. https://doi.org/10.1016/j.cub.2018.10.002.
Schenck, A., Bardoni, B., Langmann, C., Harden, N., Mandel, J.L., Giangrande, A., 2003. CYFIP/Sra-1 controls neuronal connectivity in Drosophila and links the Rac1 GTPase pathway to the fragile X protein. Neuron 38 (6), 887–898. https://doi.org/10.1016/s0896-6273(03)00354-4.
Schenck, A., Bardoni, B., Moro, A., Bagni, C., Mandel, J.L., 2001. A highly conserved protein family interacting with the fragile X mental retardation protein (FMRP) and displaying selective interactions with FMRP-related proteins FXR1P and FXR2P. Proc. Natl. Acad. Sci. U. S. A 98 (15), 8844–8849. https://doi.org/10.1073/pnas.151231598.
Schindelin, J., Arganda-Carreras, I., Frise, E., Kaynig, V., Longair, M., Pietzsch, T., Preibisch, S., Rueden, C., Saalfeld, S., Schmid, B., Tinevez, J.-Y., White, D.J., Hartenstein, V., Eliceiri, K., Tomancak, P., Cardona, A., 2012. Fiji: an open-source platform for biological-image analysis. Nat. Methods 9 (7), 676–682. https://doi.org/10.1038/nmeth.2019.
Shtrichman, R., Germanguz, I., Mandel, R., Ziskind, A., Nahor, I., Safran, M., Osenberg, S., Sherf, O., Rechavi, G., Itskovitz-Eldor, J., 2012. Altered A-to-I RNA editing in human embryogenesis. PLoS One 7 (7), e41576. https://doi.org/10.1371/journal.pone.0041576.
Snyder, E.M., Philpot, B.D., Huber, K.M., Dong, X., Fallon, J.R., Bear, M.F., 2001. Internalization of ionotropic glutamate receptors in response to mGluR activation. Nat. Neurosci. 4 (11), 1079–1085. https://doi.org/10.1038/nn746.
Varadi, M., Anyango, S., Deshpande, M., Nair, S., Natassia, C., Yordanova, G., Yuan, D., Stroe, O., Wood, G., Laydon, A., Žídek, A., Green, T., Tunyasuvunakool, K., Petersen, S., Jumper, J., Clancy, E., Green, R., Vora, A., Lutfi, M., et al., 2022. AlphaFold protein structure database: massively expanding the structural coverage of protein-sequence space with high-accuracy models. Nucleic Acids Res. 50 (D1), D439–D444. https://doi.org/10.1093/nar/gkab1061.
Xie, S., Zuo, K., De Rubeis, S., Ruggerone, P., Carloni, P., 2025. Molecular basis of the CYFIP2 and NCKAP1 autism-linked variants in the WAVE regulatory complex. Protein Sci.: Public. Protein Soc. 34 (1), e5238. https://doi.org/10.1002/pro.5238.
Yan, Y., Tao, H., He, J., Huang, S.-Y., 2020. The HDOCK server for integrated protein-protein docking. Nat. Protoc. 15 (5), 1829–1852. https://doi.org/10.1038/s41596-020-0312-x.
Zhang, Y., Kang, H., Lee, Y., Kim, Y., Lee, B., Kim, J.Y., Jin, C., Kim, S., Kim, H., Han, K., 2018. Smaller body size, early postnatal lethality, and cortical extracellular matrix-related gene expression changes of Cyfip2-Null embryonic mice. Front. Mol. Neurosci. 11, 482. https://doi.org/10.3389/fnmol.2018.00482.
Zhang, Y., Kang, H.R., Han, K., 2019a. Differential cell-type-expression of CYFIP1 and CYFIP2 in the adult mouse hippocampus. Anim. Cell Syst. 23 (6), 380–383. https://doi.org/10.1080/19768354.2019.1696406.
Zhang, Y., Lee, Y., Han, K., 2019b. Neuronal function and dysfunction of CYFIP2: from actin dynamics to early infantile epileptic encephalopathy. BMB Rep. 52 (5), 304–311. https://doi.org/10.5483/BMBRep.2019.52.5.097.
Zweier, M., Begemann, A., McWalter, K., Cho, M.T., Abela, L., Banka, S., Behring, B., Berger, A., Brown, C.W., Carneiro, M., Chen, J., Cooper, G.M., Deciphering Developmental Disorders (DDD) Study, Finnila C.R., Guillen Sacoto M.J., Henderson A., Hüffmeier U., Joset P., Kerr B., Lesca G., Leszinski G.S., McDermott J.H., Meltzer M.R., Monaghan K.G., Mostafavi R., Õunap K., Plecko B., Powis Z., Purcarin G., Reimand T., Riedhammer K.M., Schreiber J.M., Sirsi D., Wierenga K.J., Wojcik M.H., Papuc S.M., Steindl K., Sticht H., Rauch A., 2019. Spatially clustering de novo variants in CYFIP2, encoding the cytoplasmic FMRP interacting protein 2, cause intellectual disability and seizures. Eur. J. Hum. Genet.: EJHG (Eur. J. Hum. Genet.) 27 (5), 747–759. https://doi.org/10.1038/s41431-018-0331-z.